Bilayer t-J-$J_\perp$ Model and Magnetically Mediated Pairing in the Pressurized Nickelate $La_3Ni_2O_7$

Xing-Zhou Qu,[1,2,*] Dai-Wei Qu,[1,2,*] Jialin Chen,[2,3,*] Congjun Wu,[4,5,6,7] Fan Yang,[8] Wei Li,[2,3,9,†] and Gang Su[1,9,‡]
[1]Kavli Institute for Theoretical Sciences, University of Chinese Academy of Sciences, Beijing 100190, China
[2]CAS Key Laboratory of Theoretical Physics, Institute of Theoretical Physics, Chinese Academy of Sciences, Beijing 100190, China
[3]Hefei National Laboratory, Hefei 230088, China
[4]New Cornerstone Science Laboratory, Department of Physics, School of Science, Westlake University, 310024 Hangzhou, China
[5]Institute for Theoretical Sciences, Westlake University, 310024 Hangzhou, China
[6]Key Laboratory for Quantum Materials of Zhejiang Province, School of Science, Westlake University, Hangzhou 310024, Zhejiang, China
[7]Institute of Natural Sciences, Westlake Institute for Advanced Study, 310024 Hangzhou, China
[8]School of Physics, Beijing Institute of Technology, Beijing 100081, China
[9]CAS Center for Excellence in Topological Quantum Computation, University of Chinese Academy of Sciences, Beijing 100190, China

(Received 1 August 2023; accepted 19 December 2023; published 19 January 2024)

The recently discovered nickelate superconductor $La_3Ni_2O_7$ has a high transition temperature near 80 K under pressure, providing an additional avenue for exploring unconventional superconductivity. Here, with state-of-the-art tensor-network methods, we study a bilayer t-J-$J_\perp$ model for $La_3Ni_2O_7$ and find a robust s-wave superconductive (SC) order mediated by interlayer magnetic couplings. Large-scale density matrix renormalization group calculations find algebraic pairing correlations with Luttinger parameter $K_{SC} \lesssim 1$. Infinite projected entangled-pair state method obtains a nonzero SC order directly in the thermodynamic limit, and estimates a strong pairing strength $\bar{\Delta}_z \sim \mathcal{O}(0.1)$. Tangent-space tensor renormalization group simulations elucidate the temperature evolution of SC pairing and further determine a high SC temperature $T_c^*/J \sim \mathcal{O}(0.1)$. Because of the intriguing orbital selective behaviors and strong Hund's rule coupling in the compound, t-J-$J_\perp$ model has strong interlayer spin exchange (while negligible interlayer hopping), which greatly enhances the SC pairing in the bilayer system. Such a magnetically mediated pairing has also been observed recently in the optical lattice of ultracold atoms. Our accurate and comprehensive tensor-network calculations reveal a robust SC order in the bilayer t-J-$J_\perp$ model and shed light on the pairing mechanism of the high-T_c nickelate superconductor.

DOI: 10.1103/PhysRevLett.132.036502

Introduction.—High-T_c superconductivity, since its discovery in doped cuprates [1–3], has raised long-lasting research interests. Very recently, under a high pressure of above 14 GPa, a Ruddlesden-Popper bilayer perovskite $La_3Ni_2O_7$ exhibits a high T_c near 80 K [4]. Later on, optical measurements show that the compound features strong electronic correlations that place it in the proximity of a Mott phase [5], despite certain density-wave-like order under ambient pressure. Zero resistance and strange metal behaviors have been reported under high pressure by other experimental groups [6,7]. Currently, the electronic structure, effective model, and pairing mechanism in the pressurized nickelate $La_3Ni_2O_7$ are under very active investigation [8–17].

A bilayer two-orbital Hubbard model has been proposed to describe the high-pressure phase of $La_3Ni_2O_7$, where the kinetic part is determined from the density functional theory calculations [8], and the interactions including the Hubbard U, Hund's rule coupling J_H, etc., can be included. The SC instability and related pairing symmetry have been discussed with weak (to intermediate) coupling approaches [10–12]. Nevertheless, the large Coulomb interaction $U/t \gg 1$ in $La_3Ni_2O_7$ urgently calls for analysis from a strong coupling approach [13–15]. Precision many-body calculations are required to scrutinize the possible SC order in the effective model [16]. The tensor-network methods constitute a powerful and versatile approach for both ground-state [18–23] and finite-temperature properties [24–28] of correlated electrons. Unfortunately, the original bilayer two-orbital model poses great challenges to tensor-network calculations and a dimension reduction in local Hilbert space while retaining the essence of electron correlations in the nickelate is very necessary.

Lately it is proposed that by considering the orbital selective behaviors of localized d_{z^2} and itinerant $d_{x^2-y^2}$ electrons, together with the strong ferromagnetic (FM) Hund's rule coupling, a bilayer t-J-$J_\perp$ model with strong antiferromagnetic (AF) interlayer exchange $J_\perp$ may provide an adequate effective model for $La_3Ni_2O_7$ [17]. Here, we perform high-precision ground-state and finite-temperature

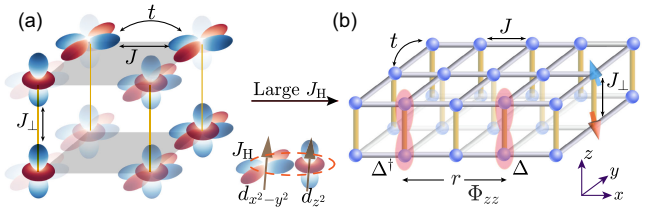

FIG. 1. (a) Two e_g orbitals in the bilayer structure of the nickelate $La_3Ni_2O_7$. The quarter-filled $d_{x^2-y^2}$ orbitals form an effective t-J model with intralayer hopping t and spin exchange J. The d_{z^2} orbital is localized and has an interlayer AF exchange through the σ bonding. The spins of $d_{x^2-y^2}$ and d_{z^2} orbitals are coupled through an on-site FM Hund's rule coupling J_H. In the large J_H limit, we arrive at (b) bilayer t-J-$J_\perp$ model, where the interlayer AF coupling $J_\perp$ is strong while the interlayer hopping is absent. The SC pairing correlation $\Phi_{zz}(r)$ is between two interlayer pairing $\Delta^{(\dagger)}$ along the vertical z direction and separated by a distance r along the x direction.

tensor-network calculations of this bilayer model, and reveal a robust SC order with high T_c that may account for the observation in the pressurized nickelate $La_3Ni_2O_7$.

Bilayer t-J-$J_\perp$ model.—As shown in Fig. 1, we note the two e_g orbitals in $La_3Ni_2O_7$, namely, $d_{x^2-y^2}$ and d_{z^2}, have distinct and orbital selective behaviors [9]. The d_{z^2} orbital is almost localized with flat band structure promoted by the strong Hund's couplings [14]. Considering that d_{z^2} orbital is only slightly doped (nearly half-filled) [13–15], we can freeze their charge fluctuations and regard the d_{z^2} electrons as local moments [14]. The interlayer σ bonding through the apical oxygen [4] renders a prominent interlayer AF coupling between the d_{z^2} moments (also dubbed as the "hidden dimer" [9]). On the other hand, the $d_{x^2-y^2}$ orbital is quarter-filled and adequately described by a t-J model within each layer [10,12,15]. The $d_{x^2-y^2}$ orbital has negligible interlayer single-particle tunneling [8,9]. However, the strong FM Hund's coupling can bind the two e_g orbitals and "passes" the strong interlayer AF coupling to the $d_{x^2-y^2}$ orbital [17], as illustrated in Fig. 1(a).

To see that, we start with the model $H = H_{t-J} + H_{\mathrm{AF}} + H_{\mathrm{Hund}}$, where H_{t-J} is the intralayer t-J model of $d_{x^2-y^2}$ electrons, and H_{AF} denotes the AF exchange $H_{\mathrm{AF}} = J_\perp \sum_i \mathbf{S}^d_{i,\mu=1} \cdot \mathbf{S}^d_{i,\mu=-1}$ between the two layers. The index $\mu = \pm 1$ labels the upper(lower) layer, and $\mathbf{S}^d$ denotes the localized d_{z^2} moment. $H_{\mathrm{Hund}} = -J_H \sum_{i,\mu} \mathbf{S}^c_{i,\mu} \cdot \mathbf{S}^d_{i,\mu}$ is the on-site Hund's coupling, with $\mathbf{S}^c$ the spin of $d_{x^2-y^2}$ electron. To further simplify the two-orbital model, it is noted that the density functional theory calculations suggest $t \simeq 0.5$ eV ($d_{x^2-y^2}$), $t^z_\perp \simeq 0.64$ eV (d_{z^2}) [8,9], placing the nickelate in the strong coupling regime by taking Hubbard $U \simeq 5$ eV (i.e., $U/t \sim 10$) [13,14]. As an intra-atomic exchange, the FM Hund's rule coupling is about $J_H \sim 1$ eV [13,14], clearly greater than the spin exchanges $J \sim 4t^2/U \simeq 0.2$ eV and $J_\perp \simeq 0.32$ eV, which is sufficiently strong to transfer the AF couplings between the two e_g orbitals [29]. It is therefore sensible to take the large J_H limit and symmetrize the spins $\mathbf{S}^d_{i,\mu}$ and $\mathbf{S}^c_{i,\mu}$ of the two orbitals. The AF interlayer coupling between d_{z^2} moments can be effectively expressed as $\mathbf{S}^c_{i,\mu=1} \cdot \mathbf{S}^c_{i,\mu=-1}$ in the symmetrized spin-triplet space. With this, an effective single-band bilayer t-J-$J_\perp$ model can be obtained [17]

$$\begin{aligned} H_{\mathrm{bilayer}} = & -t \sum_{\langle i,j\rangle,\mu,\sigma} (c^\dagger_{i,\mu,\sigma} c_{j,\mu,\sigma} + \mathrm{H.c.}) \\ & + J \sum_{\langle i,j\rangle,\mu} \left(\mathbf{S}^c_{i,\mu} \cdot \mathbf{S}^c_{j,\mu} - \frac{1}{4} n_{i,\mu} n_{j,\mu} \right) \\ & + J_\perp \sum_i \mathbf{S}^c_{i,\mu=1} \cdot \mathbf{S}^c_{i,\mu=-1}, \end{aligned} \tag{1}$$

where $\sigma = \{\uparrow, \downarrow\}$ is the spin orientation, and the vector operator $\mathbf{S}^c_{i,\mu} = \frac{1}{2} c^\dagger_{i,\mu,\sigma} (\boldsymbol{\sigma}_{\sigma,\sigma'}) c_{i,\mu,\sigma'}$ denotes the spin of the itinerant $d_{x^2-y^2}$ electron with the Pauli matrices $\boldsymbol{\sigma} = \{\sigma_x, \sigma_y, \sigma_z\}$. Note the double occupancy is projected out in the t-J-$J_\perp$ model as usual.

Below we consider the intralayer hopping $t = 3$ and spin exchange $J = 1$ (taken as energy scale henceforth), and the interlayer AF couplings $J_\perp$ is varied to explore the SC and possibly competing change density wave (CDW) orders. Interlayer hopping $t_\perp$ is forbidden [except in Fig. 3(c)], different from the previously studied bilayer Hubbard-like models [30]. As the $d_{x^2-y^2}$ orbitals are nearly quarter-filled, we set $n_e = 0.5$ and the hole density $n_h = 1 - n_e = 0.5$ in the pristine $La_3Ni_2O_7$.

Tensor-network methods for zero- and finite-temperature properties.—To simulate the bilayer model in Eq. (1), we employ tensor-network approaches for both $T = 0$ and $T > 0$ calculations. Regarding the ground state, we exploit the density matrix renormalization group (DMRG) [18,19] for the finite-size systems and the infinite projected entangled-pair state (iPEPS) directly in the thermodynamic limit [20–23]. In DMRG we map the $2 \times W \times L$ bilayer system into a quasi-1D chain with long-range interactions [31], and implement the non-Abelian and Abelian symmetries with tensor libraries [37–40]. We retain up to $D^* = 12\,000$ $\mathrm{U(1)_{charge} \times SU(2)_{spin}}$ multiplets (equivalently $D \simeq 30\,000$ individual states), which well converge the results [31]. For iPEPS calculations, we adopt the simple update [41,42] with retained bond dimension up to $D = 12$, which is extrapolated to infinite D and compared to the DMRG results. Moreover, we exploit the finite-T tensor networks, in particular the recently developed tangent-space tensor renormalization group [26] to study the bilayer system with $W = 1$ and length up to $L = 128$. Up to $D^* = 1600$ $\mathrm{U(1)_{charge} \times SU(2)_{spin}}$ multiplets (equivalently $D \simeq 3600$ states) render very well converged results down to a low temperature $T/J \simeq 0.1$ [31].

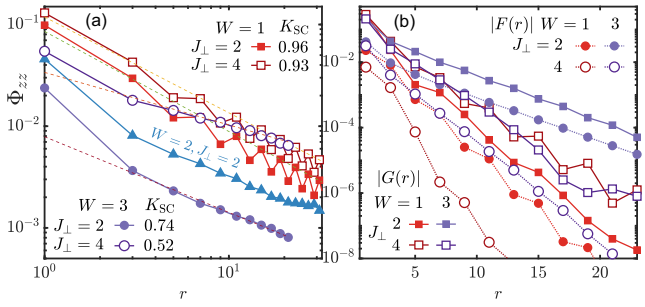

FIG. 2. (a) Pairing correlation Φ_{zz} on the $2 \times W \times L$ bilayer lattices with widths $1 \le W \le 3$ and long length L, namely, $2 \times 1 \times 128$ ($W = 1$, $n_e = 0.5$), $2 \times 2 \times 64$ ($W = 2$, $n_e \approx 0.54$), and $2 \times 3 \times 48$ ($W = 3$, $n_e = 0.5$). The SC correlations exhibit algebraic behaviors as $\Phi_{zz}(r) \sim r^{-K_{SC}}$, enhanced with interlayer coupling $J_\perp$. The $W = 2$ data fall into algebraic scaling with oscillations [31], leading to inaccurate extraction of the Luttinger parameters. (b) Spin-spin correlation $F(r)$ and the single-particle Green's function $G(r)$ decay exponentially (see definitions in the main text) in the SC phase [44].

Robust SC order and magnetically mediated interlayer pairing.—In Fig. 2 we show the DMRG results of pairing correlations $\Phi_{zz}(r) = \langle \Delta_i^\dagger \Delta_j \rangle$ with interlayer pairing $\Delta_i^\dagger = (1/\sqrt{2}) \sum_{\mu=\pm 1} c^\dagger_{i,\mu,\uparrow} c^\dagger_{i,-\mu,\downarrow}$ and distance $r \equiv |j - i|$, where we find $\Phi_{zz}(r)$ shows algebraic scaling with the Luttinger exponent $K_{SC} \lesssim 1$ for moderate to strong $J_\perp$. In Fig. 2(b), we calculate the spin-spin correlation $F(r) = \frac{1}{2} \sum_\mu \langle \mathbf{S}^c_{i,\mu} \cdot \mathbf{S}^c_{j,\mu} \rangle$ and the Green's function $G(r) = \frac{1}{4} \sum_{\mu,\sigma} \langle c^\dagger_{i,\mu,\sigma} c_{j,\mu,\sigma} + \text{H.c.} \rangle$, and find both correlations decay exponentially. The DMRG results in Fig. 2 indicate the emergence of Luther-Emery liquid [43] with quasi-long-range SC order, as well as finite spin and single-particle gaps.

The AF exchange $J_\perp$ plays an essential role in mediating the interlayer pairing and forming the rung-singlet SC phase [45]. In Fig. 3(a), we provide the DMRG results of the Luttinger parameter K_{SC} controlling the scaling behaviors of pairing correlations. We find $(2 - K_{SC}) \gtrsim 1$ increases rapidly with $J_\perp$ and signifies a diverging susceptibility at low temperature as $\chi_{SC} \sim 1/T^{(2-K_{SC})}$. The pairing susceptibility $\chi_{SC} = (2/N) \partial \langle \Delta_{tot} \rangle_\beta / \partial h_p$ measures the response of SC order parameter to a small pairing field h_p coupled to $\Delta_{tot} = \frac{1}{2} \sum_i (\Delta_i + \Delta_i^\dagger)$. To further characterize the enhancement of pairing strength, we compute the binding energy $E_b = E(N_e + 1) + E(N_e - 1) - 2E(N_e)$, where $E(N_e)$ is the ground-state energy with N_e electrons. In Fig. 3(a), we find E_b increases with $J_\perp$ as the ratio $E_b/J_\perp \gtrsim 0.6$. However, $E_b/J_\perp$ is not monotonic and has a round peak at $J_\perp \approx 1.5$. In the strong $J_\perp$ limit the escalation of binding energy slows down its pace and the ratio converges to $E_b/J_\perp \simeq 0.6$.

With iPEPS calculations directly in the thermodynamic limit where symmetry breaking is allowed to occur,

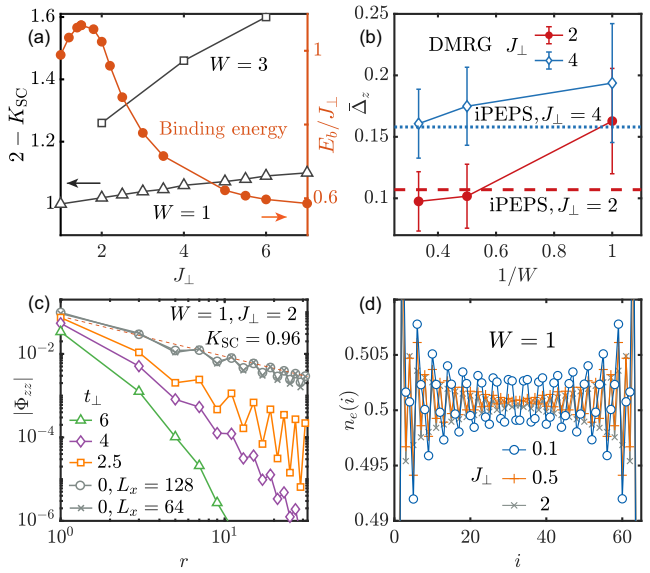

FIG. 3. (a) The Luttinger parameter $(2 - K_{SC})$ vs $J_\perp$ calculated on various bilayer systems. The binding energy for $W = 1$ system is also shown. (b) The SC order parameter $\bar{\Delta}_z$ obtained with iPEPS (dashed horizontal lines) and DMRG (solid lines) for $J_\perp = 2, 4$. In the latter, $\bar{\Delta}_z$ is estimated within central columns, and the error bars represent the difference between the maximal and minimal values by varying the number of columns involved. We set $n_e = 0.5$ for the $W = 1, 3$ cases, while for the $W = 2$ case it is shifted slightly to $n_e \simeq 0.54$. (c) Pairing correlation $|\Phi_{zz}|$ with various interlayer hopping $t_\perp$. For the $t_\perp = 0$ case, we show the pairing correlations in excellent data convergence as computed with $L_x = 64$ and 128. (d) The electron density profiles $n_e(i)$, $1 \le i \le L$ for various $J_\perp$ computed on the $2 \times 1 \times 64$ system.

we evaluate the SC order parameter $\bar{\Delta}_z = \langle \Delta_i^{(\dagger)} \rangle$ averaged over the two sublattices, and show the results in Fig. 3(b). We find $\bar{\Delta}_z$ increases with $J_\perp$ and reaches about 0.11 for $J_\perp = 2$ and 0.16 for $J_\perp = 4$. In Fig. 3(b) we also show the DMRG estimation of the order parameter $\bar{\Delta}_z = \sqrt{(1/N_b) \sum_{i,j} \langle \Delta_i^\dagger \Delta_j \rangle}$ where i, j are restricted within N_c central columns, and N_b is number of the credited pairs. In practice, we vary N_c from 8 to 16 for different lattice geometries, and find the DMRG and iPEPS results agree well. Notice that the order parameter $\bar{\Delta}_z$ of the bilayer t-J-$J_\perp$ system [$\mathcal{O}(10^{-1})$] is much greater than that found in the plain t-J square lattice [$\mathcal{O}(10^{-2})$] [46].

The order parameter $\bar{\Delta}_z$ and pairing correlations are found to be uniform in each layer, i.e., it belongs to an s-wave SC order. We have also computed the intralayer pairings with DMRG, and the order parameters with iPEPS [31], which are found to be negligibly small when compared to Φ_{zz} (and $\bar{\Delta}_z$). Based on the results in Figs. 2 and 3, we conclude there exists a robust rung-singlet SC order mediated and enhanced by magnetic couplings $J_\perp$ in the bilayer t-J-$J_\perp$ model for $La_3Ni_2O_7$.

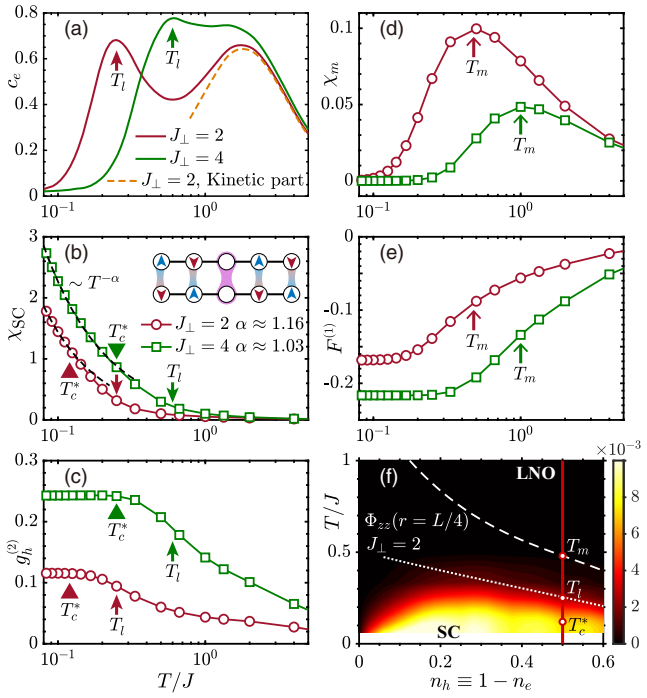

FIG. 4. Finite-temperature results for $W = 1$ systems with length up to $L = 128$. In panels (a)–(e), the data for $J_\perp = 2$ (red lines) and 4 (green) are shown. In (a),(c)–(e) the hole density is fixed as $n_h \equiv 1 - n_e = 0.5$, and in (b) the data are calculated with fine-tuned chemical potential that leads to $n_h \simeq 0.5$. (a) Shows the specific heat c_e with T_l the lower characteristic temperature. (b) Shows the pairing susceptibility $\chi_{\rm SC}$, which diverges with a power-law scaling $T^{-\alpha}$ (the dashed lines) for $T \le T_c^*$. The interlayer pairing and AF correlations are illustrated in the inset. (c) Shows the interlayer hole correlations on the rungs, with T_l and T_c^* determined from (a) and (b), respectively. (d) Shows the magnetic susceptibility χ_m with a hump at T_m. (e) Shows the rung spin correlations. (f) The contour plot of the pairing correlation $\Phi_{zz}(r = L/4)$ for various hole densities n_h computed with $J_\perp = 2$. The vertical red line denotes the $n_h = 0.5$ case relevant for $La_3Ni_2O_7$ (LNO).

Pauli blocking and charge density-wave instability.—The existence of strong interlayer $J_\perp$ while absence of hopping $t_\perp$ is a key for the robust SC order to appear in the bilayer system. In Fig. 3(c) we artificially introduce the interlayer hopping $t_\perp$, and find the SC order gets weakened and even suppressed as $t_\perp$ increases. This can be ascribed to the Pauli blocking effect where the holes tend to repel each other kinetically according to their hopping amplitude [47], spoiling the interlayer pairing for strong $t_\perp$. Moreover, this observation may also be relevant to the experiments: further increasing pressure in the SC phase of $La_3Ni_2O_7$ does not enhance T_c but decreases it [4,6,7]. It is possible that high pressure enhances interlayer tunneling of the $d_{x^2-y^2}$ orbitals and thus weakens the SC order.

In Fig. 3(d), we show the electron density distribution $n_e(i)$ by tuning $J_\perp$ to smaller values. For $J_\perp = 2$, the CDW fluctuation is rather weak, consistent with a robust s-wave SC state. However, for smaller $J_\perp$ the SC order becomes weakened, while the CDW instability turns strong. This may explain the absence of SC order in $La_3Ni_2O_7$ under ambient pressure, where certain density-wave-like instability bas been observed in recent experiments [5–7]. The change of interlayer Ni-O-Ni bond angle [from 168° (ambient) to 180° (pressurized)] and length (by 1.9 Å) may sensitively influence $J_\perp$, thus switching between the CDW and SC phases. Moreover, by reducing the hole density we find even clearer CDW pattern [31], suggesting that the CDW instability or stripe phase may also be a competing order in the bilayer nickelate.

Finite-temperature pairing and magnetic susceptibilities.—In Fig. 4 we show the temperature evolutions of spin and pairing correlations. Firstly, from Fig. 4(a) we find the electron specific heat $c_e = (1/N_e)(\partial\varepsilon/\partial T)$ exhibits a double-peak structure, with the higher-T peak contributed by the kinetic energy, and lower-T scale responsible for SC pairing labeled by T_l. In Fig. 4(b) we apply a uniform pairing field $-h_p\Delta_{\rm tot}$ with $h_p = 2 \times 10^{-3}$, and compute the pairing susceptibility. We find that $\chi_{\rm SC}$ is rather small for $T > T_l$ and becomes significant for $T < T_l$, making T_l the SC-fluctuation onset temperature.

As temperature further lowers, we find $\chi_{\rm SC}$ exhibits an algebraic divergence $\chi_{\rm SC} \sim T^{-\alpha}$ for temperature below T_c^*, when the system enters the low-temperature SC regime. The fitted exponent in Fig. 4(b) is $\alpha \simeq 1$, consistent with the ground-state DMRG results of $K_{\rm SC} \simeq 1$ for $W = 1$. Both T_l and T_c^* increase with $J_\perp$, and in Fig. 4(a) we find $T_l/J \simeq 0.25$ for $J_\perp = 2$, which is enhanced to $T_l/J \simeq 0.6$ for $J_\perp = 4$. Similarly in Fig. 4(b) the $\chi_{\rm SC}$ curves show an overall enhancement, and the T_c^*/J increases from 0.12 for $J_\perp = 2$ to about 0.25 for $J_\perp = 4$. In Fig. 4(c) we show the hole-hole correlation $g_h^{(2)} = (2/N)\sum_i \langle h_{i,\mu=1} h_{i,\mu=-1}\rangle_\beta \cdot \langle h_{i,\mu=-1}\rangle_\beta) - 1$ where N is the number of lattice sites with $h_{i,\mu}$ the hole density operator. The positive $g_h^{(2)}$ indicates the attractive ("bunching") correlations between the holes. From Fig. 4(c), we find $g_h^{(2)}$ rapidly increases at about T_l and saturates at about T_c^* when the pairing susceptibility starts to diverge algebraically in Fig. 4(b).

To further reveal the intriguing interplay between antiferromagnetism and superconductivity in the bilayer system, we compute the magnetic susceptibility χ_m and rung spin-spin correlation $F^{(1)} = (2/N)\sum_i \langle \mathbf{S}_{i,\mu=1} \cdot \mathbf{S}_{i,\mu=-1}\rangle_\beta$ in Figs. 4(d) and 4(e). The magnetic susceptibility χ_m becomes suppressed below T_m in Fig. 4(d), which can be ascribed to the rapid establishment of correlation $F^{(1)}$ at about the same temperature [Fig. 4(e)].

Temperature evolution of the SC order.—Now we summarize the temperature evolution of the pairing correlations in Fig. 4(f), where the red line denotes $La_3Ni_2O_7$ with hole density $n_h \equiv 1 - n_e \simeq 0.5$. As temperature lowers, the interlayer AF correlation develops at about $T_m/J \simeq 0.48$, and then the hole bunching occurs at $T_l/J \simeq 0.25$, shortly after that the system enters the

coherent regime below $T_c^*/J \simeq 0.12$, establishing eventually the quasi-long-range SC order.

As shown in Fig. 4(f), by doping electrons into the system (or via a self-doping from d_{z^2} to the $d_{x^2-y^2}$ orbitals), the SC order and its characteristic temperature can be further enhanced. For $J_\perp = 2$, the optimal hole density appears at $n_h \sim 0.25$, to the electron-doping side of $La_3Ni_2O_7$, as also evidenced by the enhanced pairing susceptibility and temperature scales T_l and T_c^* [31].

Discussion and outlook.—We exploit multiple tensor-network methods and reveal robust *s*-wave SC order in the bilayer t-J-$J_\perp$ model for the recently discovered nickelate superconductor. In $La_3Ni_2O_7$ the $d_{x^2-y^2}$ orbital has a hole density of $n_h \simeq 0.5$—a large value on the verge of quenching the SC in cuprates. For the latter, large hole doping may undermine the intralayer AF correlations and suppress the SC order. Surprisingly, in $La_3Ni_2O_7$ the SC order remains robust and has a high $T_c \simeq 80$ K even with large hole density. Based on our t-J-$J_\perp$ model calculations, we ascribe it to the robust pairing mechanism mediated by strong interlayer AF exchange. In Fig. 4(f), we find indeed the SC dome can extend to a very wide regime up to $n_h \sim 0.6$ for the bilayer nickelate.

We would also point out an intriguing and rather unexpected connection between the high-T_c nickelate and ultracold atom systems. Recently, the mixed dimensional (mixD) bilayer optical lattices with strong interlayer spin exchange while no interlayer single-particle tunneling has been realized [47,48]. Remarkably, such a t-J-$J_\perp$ mixD bilayer model naturally emerges in the orbital-selective nickelate $La_3Ni_2O_7$: The $d_{x^2-y^2}$ electrons are itinerant within each layer, while d_{z^2} orbitals are nearly half-filled and localized. The FM Hund's coupling "glues" the spins of two e_g orbitals, conveying to the $d_{x^2-y^2}$ electrons a strong AF coupling—the driving force for the interlayer pairing. To thoroughly validate our effective model for $La_3Ni_2O_7$, a detailed analysis of the two-orbital bilayer model with realistic parameters is necessary. Our preliminary results support the scenario proposed here [29].

Overall, our results provide a solid and valuable basis for understanding the unconventional SC in pressurized $La_3Ni_2O_7$ from a strong coupling approach, and put various experimental observations in a coherent picture. They offer useful guidance for future studies in the nickelate superconductors and also mixD ultracold atom systems.

W. L. and F. Y. are indebted to Yang Qi and Qiaoyi Li for stimulating discussions. This work was supported by the National Natural Science Foundation of China (Grants No. 12222412, No. 11834014, No. 11974036, No. 12047503, No. 12074031, No. 12174317, and No. 12234016), Strategic Priority Research Program of CAS (Grant No. XDB28000000), Innovation Program for Quantum Science and Technology (No. 2021ZD0301800 and No. 2021ZD0301900), the New Cornerstone Science Foundation, and CAS Project for Young Scientists in Basic Research (Grant No. YSBR-057). We thank the HPC-ITP for the technical support and generous allocation of CPU time.

*These authors contributed equally to this work.
†Corresponding author: w.li@itp.ac.cn
‡Corresponding author: gsu@ucas.ac.cn

[1] J. G. Bednorz and K. A. Müller, Possible high-T_c superconductivity in the Ba-La-Cu-O system, Z. Phys. B Condens. Matter **64**, 189 (1986).
[2] P. A. Lee, N. Nagaosa, and X.-G. Wen, Doping a mott insulator: Physics of high-temperature superconductivity, Rev. Mod. Phys. **78**, 17 (2006).
[3] B. Keimer, S. A. Kivelson, M. R. Norman, S. Uchida, and J. Zaanen, From quantum matter to high-temperature superconductivity in copper oxides, Nature (London) **518**, 179 (2015).
[4] H. Sun, M. Huo, X. Hu, J. Li, Z. Liu, Y. Han, L. Tang, Z. Mao, P. Yang, B. Wang, J. Cheng, D.-X. Yao, G.-M. Zhang, and M. Wang, Signatures of superconductivity near 80 K in a nickelate under high pressure, Nature (London) **621**, 493 (2023).
[5] Z. Liu, M. Huo, J. Li, Q. Li, Y. Liu, Y. Dai, X. Zhou, J. Hao, Y. Lu, M. Wang, and H.-H. Wen, Electronic correlations and energy gap in the bilayer nickelate $La_3Ni_2O_7$, arXiv:2307.02950.
[6] J. Hou, P. T. Yang, Z. Y. Liu, J. Y. Li, P. F. Shan, L. Ma, G. Wang, N. N. Wang, H. Z. Guo, J. P. Sun, Y. Uwatoko, M. Wang, G. M. Zhang, B. S. Wang, and J. G. Cheng, Emergence of high-temperature superconducting phase in the pressurized $La_3Ni_2O_7$ crystals, Chin. Phys. Lett. **40**, 117302 (2023).
[7] Y. Zhang, D. Su, Y. Huang, H. Sun, M. Huo, Z. Shan, K. Ye, Z. Yang, R. Li, M. Smidman, M. Wang, L. Jiao, and H. Yuan, High-temperature superconductivity with zero-resistance and strange metal behavior in $La_3Ni_2O_7$, arXiv:2307.14819.
[8] Z. Luo, X. Hu, M. Wang, W. Wú, and D.-X. Yao, Bilayer two-orbital model of $La_3Ni_2O_7$ under pressure, Phys. Rev. Lett. **131**, 126001 (2023).
[9] Y. Zhang, L.-F. Lin, A. Moreo, and E. Dagotto, Electronic structure, orbital-selective behavior, and magnetic tendencies in the bilayer nickelate superconductor $La_3Ni_2O_7$ under pressure, Phys. Rev. B **108**, L180510 (2023).
[10] Q.-G. Yang, D. Wang, and Q.-H. Wang, Possible $s_\pm$-wave superconductivity in $La_3Ni_2O_7$, Phys. Rev. B **108**, L140505 (2023).
[11] H. Sakakibara, N. Kitamine, M. Ochi, and K. Kuroki, Possible high T_c superconductivity in $La_3Ni_2O_7$ under high pressure through manifestation of a nearly-half-filled bilayer Hubbard model, arXiv:2306.06039.
[12] Y. Gu, C. Le, Z. Yang, X. Wu, and J. Hu, Effective model and pairing tendency in bilayer Ni-based superconductor $La_3Ni_2O_7$, arXiv:2306.07275.
[13] V. Christiansson, F. Petocchi, and P. Werner, Correlated electronic structure of $La_3Ni_2O_7$ under pressure, Phys. Rev. Lett. **131**, 206501 (2023).

[14] Y. Cao and Y.-F. Yang, Flat bands promoted by Hund's rule coupling in the candidate double-layer high-temperature superconductor $La_3Ni_2O_7$, arXiv:2307.06806.
[15] W. Wú, Z. Luo, D.-X. Yao, and M. Wang, Charge transfer and Zhang-Rice singlet bands in the nickelate superconductor $La_3Ni_2O_7$ under pressure, arXiv:2307.05662.
[16] Y. Shen, M. Qin, and G.-M. Zhang, Effective bi-layer model Hamiltonian and density-matrix renormalization group study for the high-T_c superconductivity in $La_3Ni_2O_7$ under high pressure, Chin. Phys. Lett. **40**, 127401 (2023).
[17] C. Lu, Z. Pan, F. Yang, and C. Wu, Interlayer coupling driven high-temperature superconductivity in $La_3Ni_2O_7$ under pressure, arXiv:2307.14965.
[18] S. R. White, Density matrix formulation for quantum renormalization groups, Phys. Rev. Lett. **69**, 2863 (1992).
[19] U. Schollwöck, The density-matrix renormalization group in the age of matrix product states, Ann. Phys. (Amsterdam) **326**, 96 (2011).
[20] F. Verstraete and J. I. Cirac, Renormalization algorithms for quantum-many body systems in two and higher dimensions, arXiv:cond-mat/0407066.
[21] J. I. Cirac, D. Pérez-García, N. Schuch, and F. Verstraete, Matrix product states and projected entangled pair states: Concepts, symmetries, theorems, Rev. Mod. Phys. **93**, 045003 (2021).
[22] P. Corboz, R. Orús, B. Bauer, and G. Vidal, Simulation of strongly correlated fermions in two spatial dimensions with fermionic projected entangled-pair states, Phys. Rev. B **81**, 165104 (2010).
[23] J. Jordan, R. Orús, G. Vidal, F. Verstraete, and J. I. Cirac, Classical simulation of infinite-size quantum lattice systems in two spatial dimensions, Phys. Rev. Lett. **101**, 250602 (2008).
[24] W. Li, S.-J. Ran, S.-S. Gong, Y. Zhao, B. Xi, F. Ye, and G. Su, Linearized tensor renormalization group algorithm for the calculation of thermodynamic properties of quantum lattice models, Phys. Rev. Lett. **106**, 127202 (2011).
[25] B.-B. Chen, L. Chen, Z. Chen, W. Li, and A. Weichselbaum, Exponential thermal tensor network approach for quantum lattice models, Phys. Rev. X **8**, 031082 (2018).
[26] Q. Li, Y. Gao, Y.-Y. He, Y. Qi, B.-B. Chen, and W. Li, Tangent space approach for thermal tensor network simulations of the 2D Hubbard model, Phys. Rev. Lett. **130**, 226502 (2023).
[27] B.-B. Chen, C. Chen, Z. Chen, J. Cui, Y. Zhai, A. Weichselbaum, J. von Delft, Z. Y. Meng, and W. Li, Quantum many-body simulations of the two-dimensional Fermi-Hubbard model in ultracold optical lattices, Phys. Rev. B **103**, L041107 (2021).
[28] X. Lin, B.-B. Chen, W. Li, Z. Y. Meng, and T. Shi, Exciton proliferation and fate of the topological Mott insulator in a twisted bilayer graphene lattice model, Phys. Rev. Lett. **128**, 157201 (2022).
[29] X.-Z. Qu, D.-W. Qu, W. Li, and G. Su, Roles of Hund's rule and hybridization in the two-orbital model for high-T_c superconductivity in the bilayer nickelate, arXiv:2311.12769.
[30] T. A. Maier and D. J. Scalapino, Pair structure and the pairing interaction in a bilayer Hubbard model for unconventional superconductivity, Phys. Rev. B **84**, 180513(R) (2011).
[31] See Supplemental Material at http://link.aps.org/supplemental/10.1103/PhysRevLett.132.036502 in which Sec. I introduces the many-body calculation methods, including the DMRG, iPEPS, and tanTRG exploited in this work, and Sec. II provides supplemental data for the ground-state and finite-temperature properties, which includes Refs. [32–36].
[32] X. Lu, D.-W. Qu, Y. Qi, W. Li, and S.-S. Gong, Ground-state phase diagram of the extended two-leg t-J ladder, Phys. Rev. B **107**, 125114 (2023).
[33] P. Corboz and G. Vidal, Fermionic multiscale entanglement renormalization ansatz, Phys. Rev. B **80**, 165129 (2009).
[34] T. Barthel, C. Pineda, and J. Eisert, Contraction of fermionic operator circuits and the simulation of strongly correlated fermions, Phys. Rev. A **80**, 042333 (2009).
[35] C. V. Kraus, N. Schuch, F. Verstraete, and J. I. Cirac, Fermionic projected entangled pair states, Phys. Rev. A **81**, 052338 (2010).
[36] R. Orús and G. Vidal, Simulation of two-dimensional quantum systems on an infinite lattice revisited: Corner transfer matrix for tensor contraction, Phys. Rev. B **80**, 094403 (2009).
[37] A. Weichselbaum, Non-Abelian symmetries in tensor networks: A quantum symmetry space approach, Ann. Phys. (Amsterdam) **327**, 2972 (2012).
[38] A. Weichselbaum, X-symbols for non-Abelian symmetries in tensor networks, Phys. Rev. Res. **2**, 023385 (2020).
[39] M. Fishman, S. R. White, and E. M. Stoudenmire, The ITensor software library for tensor network calculations, SciPost Phys. Codebases 4 (2022).
[40] M. Fishman, S. R. White, and E. M. Stoudenmire, Codebase release 0.3 for ITensor, SciPost Phys. Codebases 4 (2022).
[41] H. C. Jiang, Z. Y. Weng, and T. Xiang, Accurate determination of tensor network state of quantum lattice models in two dimensions, Phys. Rev. Lett. **101**, 090603 (2008).
[42] W. Li, J. von Delft, and T. Xiang, Efficient simulation of infinite tree tensor network states on the bethe lattice, Phys. Rev. B **86**, 195137 (2012).
[43] A. Luther and V. J. Emery, Backward scattering in the one-dimensional electron gas, Phys. Rev. Lett. **33**, 589 (1974).
[44] We compute the spin, charge, and SC pairing correlations on a pair of sites separated by distance r and symmetric around the center of the system to avoid boundary effects.
[45] W. Wu, M. Ferrero, A. Georges, and E. Kozik, Controlling Feynman diagrammatic expansions: Physical nature of the pseudogap in the two-dimensional Hubbard model, Phys. Rev. B **96**, 041105(R) (2017).
[46] P. Corboz, T. M. Rice, and M. Troyer, Competing states in the t-J model: Uniform d-wave state versus stripe state, Phys. Rev. Lett. **113**, 046402 (2014).
[47] S. Hirthe, T. Chalopin, D. Bourgund, P. Bojović, A. Bohrdt, E. Demler, F. Grusdt, I. Bloch, and T. A. Hilker, Magnetically mediated hole pairing in fermionic ladders of ultracold atoms, Nature (London) **613**, 463 (2023).
[48] A. Bohrdt, L. Homeier, I. Bloch, E. Demler, and F. Grusdt, Strong pairing in mixed-dimensional bilayer antiferromagnetic Mott insulators, Nat. Phys. **18**, 651 (2022).